FERMILAB-CONF-18-807-E

Prepared for submission to JINST

N[TH] Workshop on X
when
where

The Mu2e crystal calorimeter

N. Atanov[d] **J. Budagov** [d] **F. Cervelli** [c] **F. Colao**[a] **M. Cordelli**[a] **G. Corradi**[a] **E. Danè**[a] **Y. Davidov**[d] **S. Di Falco**[c] **E. Diociaiuti**[a] **S. Donati**[b,c] **R. Donghia**[a] **B. Echenard**[e] **S. Giovannella**[a] **V. Glagolev**[d] **F. Grancagnolo**[f] **F. Happacher**[a,1] **D. Hitlin**[e] **M.Martini**[a,h] **S. Miscetti**[a] **T. Miyashita**[e] **L. Morescalchi**[c] **P. Murat**[g] **E. Pedreschi**[c] **G. Pezzullo**[c] **F. Porter**[e] **A. Saputi**[a] **I. Sarra**[a,h] **F. Spinella**[c] **G. Tassielli**[f]

[a] *INFN Laboratori Nazionali di Frascati , via Enrico Femri 40, Frascati, Italy*
[b] *Departement of Physics, University of Pisa, Largo B. Pontecorvo 3, Pisa , Italy*
[c] *INFN sezione di Pisa, Italy, Largo B. Pontecorvo 3, Pisa , Italy*
[d] *Joint Institute for Nuclear Research, Joliot-Curie 6, Dubna, Russia*
[e] *Departement of Physics, California Institute of Technology, 1200 E California Blvd, Pasadena (CA), USA*
[f] *INFN sezione di Lecce, Via Arnesano 73100, Lecce, Italy*
[g] *Fermi National Accelerator Laboratory, Main Entrance Rd, Batavia (IL), USA*
[h] *Department of Energy, University Guglielmo Marconi, via Plinio, 44, 00193 Roma, Italy*

E-mail: fabio.happacher@lnf.infn.it

[1] Corresponding author.

Abstract: The Mu2e Experiment at Fermilab will search for coherent, neutrino-less conversion of negative muons into electrons in the field of an Aluminum nucleus, $\mu^- + Al \rightarrow e^- + Al$. Data collection start is planned for the end of 2021.

The dynamics of such charged lepton flavour violating (CLFV) process is well modelled by a two-body decay, resulting in a mono-energetic electron with an energy slightly below the muon rest mass. If no events are observed in three years of running, Mu2e will set an upper limit on the ratio between the conversion and the capture rates $R_{\mu e} = \frac{\mu^- + A(Z,N) \rightarrow e^- + A(Z,N)}{\mu^- + A(Z,N) \rightarrow \nu_\mu + A(Z-1,N)}$ of $\leq 6 \times 10^{-17}$ (@ 90% C.L.).

This will improve the current limit of four order of magnitudes with respect to the previous best experiment.

Mu2e complements and extends the current search for $\mu \rightarrow e\gamma$ decay at MEG as well as the direct searches for new physics at the LHC. The observation of such CLFV process could be clear evidence for New Physics beyond the Standard Model. Given its sensitivity, Mu2e will be able to probe New Physics at a scale inaccessible to direct searches at either present or planned high energy colliders.

To search for the muon conversion process, a very intense pulsed beam of negative muons ($\sim 10^{10} \mu$/ sec) is stopped on an Aluminum target inside a very long solenoid where the detector is also located. The Mu2e detector is composed of a straw tube tracker and a CsI crystals electromagnetic calorimeter. An external veto for cosmic rays surrounds the detector solenoid. In 2016, Mu2e has passed the final approval stage from DOE and has started its construction phase.

An overview of the physics motivations for Mu2e, the current status of the experiment and the required performances and design details of the calorimeter are presented.

Keywords: Only keywords from JINST's keywords list please

ArXiv ePrint: 1234.56789

Contents

1 Charged Lepton Flavor Violation and muon to electron conversion

Within the Standard Model (SM), transitions in the lepton sector between charged and neutral particles preserve flavor, since the neutrinos are considered massless. Even considering the discovery of neutrino oscillations, in the minimal extension of SM, the predicted branching ratios of Charged Lepton Flavor Violation (CLFV) processes in the muon sector are smaller than 10^{-50}.

No CLFV process has been observed yet, so any experimental detection would be a clear signature of New Physics (NP) beyond the Standard Model. One of the most promising process for probing CLFV is the coherent muon conversion in the field of a nucleus, μ N $\rightarrow$ e N. In this process the nucleus is left intact and the resulting electron has a monochromatic energy slightly below the muon rest mass ($\sim$ 104.96 MeV for Al), due to the nucleus recoil.

The Mu2e experiment [2] is designed to improve the current limit on the conversion rate, $R_{\mu e}$, by 4 orders of magnitude over the SINDRUM II experiment [3]. $R_{\mu e}$ is defined as the ratio between the number of electrons from the conversion process and the number of captured muons:

$$R_{\mu e} = \frac{\mu^- N(Z,A) \rightarrow e^- N(Z,A)}{\mu^- N(Z,A) \rightarrow \nu_\mu N(Z-1,A)}$$

where, in the Mu2e case, N(Z,A) is an Aluminum nucleus.

Many NP scenarios, like SUSY, Leptoquarks, Heavy Neutrinos, GUT, Extra Dimensions or Little Higgs, predict significantly enhanced values for $R_{\mu e}$, allowing the detection of the process with the expected Mu2e sensitivity [4].

A model independent description of the CLFV transitions, for NP models, is provided by an effective Lagrangian [5] where the different processes are divided in dipole amplitudes and contact term operators. The $\mu \rightarrow e\gamma$ decay is mainly sensitive to the dipole amplitude, while $\mu \rightarrow e$ conversion and $\mu \rightarrow 3e$ receive contributions also from the conctact interactions. It is possible

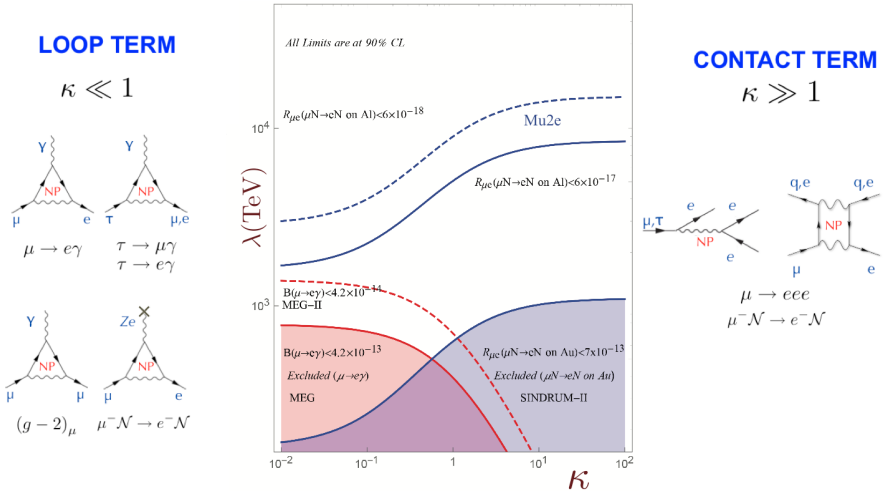

Figure 1. Sensitivity of $\mu \to e\gamma$, $\mu \to e$ transition and $\mu \to 3e$ to the scale of new physics Λ as a function of the parameter κ . The shaded areas are excluded by present limits. On the left (right) side, the dipole (four-fermion) diagrams are shown for the different processes.

to parametrise the interpolation between the two amplitudes by means of two parameters [5]: Λ, which sets the mass scale, and κ, which governs the ratio of the four fermion to the dipole amplitude. For $\kappa \ll 1 (\gg 1)$ the dipole-type (contact) operator dominates. Figure 1 summarises the power of different searches to explore this parameter space [6].

Present experimental limits already excluded lepton flavour violation up to a mass scale up of $\Lambda < 700$ TeV. The interpretation of an eventual direct observation of NP at LHC will have to take into account precise measurements (or constraints) from MEG [7] and Mu2e: the comparison between these determinations will help pinning down the underlying theory.

2 Muonic Aluminum atom

When negative muons stop in the Aluminum target, they are captured in an atomic excited state. They promptly fall to the ground state, then 39% of them decay in orbit, $\mu^- \to e^- \bar{\nu}_e \nu_\mu$ (DIO), while the remaining 61% are captured on the nucleus. Low energy photons, neutrons and protons are emitted in the nuclear capture process and constitutes an environmental background that produces a ionisation dose and a neutron fluency on the detection systems as well as an accidental occupancy for the reconstruction program.

The kinematic limit for the muon decay in vacuum is at about 54 MeV, but the nucleus recoil generates a long tail that has the endpoint exactly at the conversion electron energy.

DIO electrons are an irreducible background that have to be distinguished by the mono-energetic conversion electron (CE). The finite tracking resolution and the positive reconstruction tail has a large effect on the falling spectrum of the DIO background that translates in a residual contamination in the signal region as shown in Fig 2.

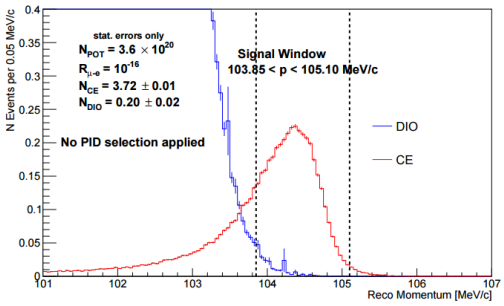

Figure 2. Full simulation of DIO and CE events for an assumed $R_{\mu e}$ of 10^{-16}.

3 The Mu2e experimental apparatus

The Mu2e apparatus consists of three superconductive solenoid magnets, as shown in Figure 3: the Production Solenoid (PS), the Transport Solenoid (TS) and the Detector Solenoid (DS).

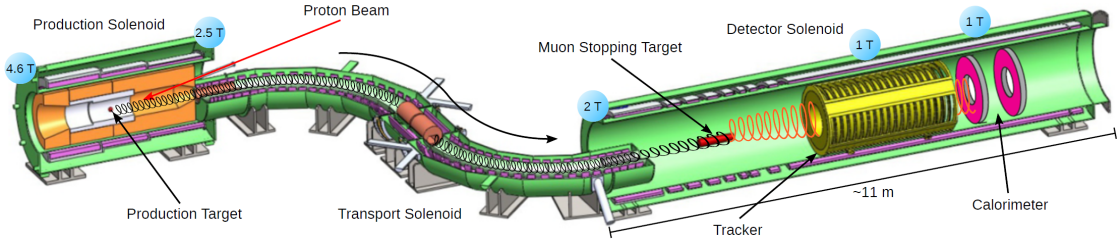

Figure 3. Layout of the Mu2e experiment.

The proton beam interacts in the PS with a tungsten target, producing mostly pions and muons. The gradient field in the PS increases from 2.5 to 4.6 T in the same direction of the incoming beam and opposite to the outgoing muon beam direction. This gradient field works as a magnetic lens to focus charged particles into the transport channel. The focused beam is constituted by muons, pions with a small contamination of protons and antiprotons. When the beam passes through the S-shaped TS, low momentum negative charged particles are selected and delivered to the Aluminum stopping targets in the DS. Electrons from the μ-conversion (CE) in the stopping target are captured by the magnetic field in the DS and transported through the Straw Tube Tracker, that reconstructs the CE trajectory and its momentum. The CE then strikes the Electromagnetic Calorimeter, that provides independent measurements of the energy, the impact time and the position. Both detectors operate in a 10^{-4} Torr vacuum and in an uniform 1 T axial field.

A Cosmic Ray Veto (CRV) system covers the entire DS and half of the TS, as shown in Figure 6 (right).

Additional details on the Mu2e apparatus can be found in [2].

4 The Mu2e Tracker and Cosmic Ray Veto

The tracking detector is made of low mass straw drift tubes oriented transversally to the solenoid axis. The detector consists of about 21000 straw tubes arranged in 18 stations, as shown in Figure 4 (left). Each tube is of 5 mm in diameter and contains a 25 μm sense wire. The straw walls are made of Mylar and have a thickness of 15 μm.

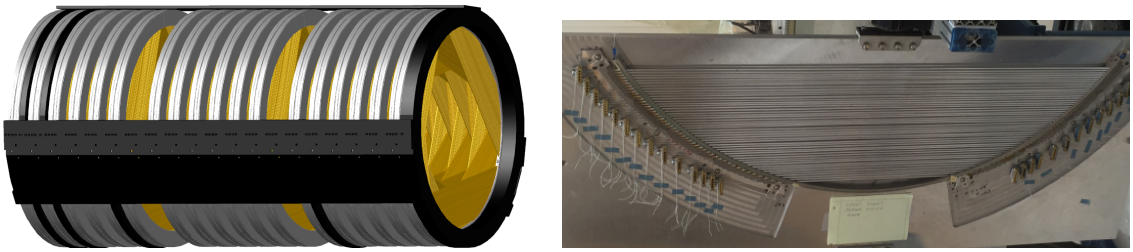

Figure 4. (Left) Sketch of the Mu2e straw tracker system. (right) Picture of the first prototype built for straw tube panel.

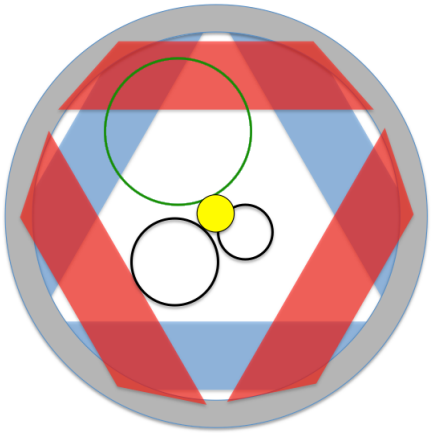

Figure 5. Transverse view of the Tracker active area. Only tracks emerging from the stopping target (yellow spot) with momentum $p > 55$ MeV/c (green circles) leave hits in the straw tubes. Lower momentum tracks (black circles) leave the detectors undetected.

The gas used is a 80:20 mixture of Argon-CO_2. The tracker is around 3 m long and measures the momenta of the charged particles from the reconstructed trajectories using the hits detected in the straw. As shown in Figure 5, a circular inner un-instrumented region inside the tracker makes it insensitive to charged particle with momenta below 55 MeV/c. Indeed its acceptance is optimised to identify $\sim$ 100 MeV electrons. Each straw tube is instrumented on both sides with TDCs to measure the particle crossing time and ADCs to measure the specific energy loss dE/dX used to separate electrons from highly ionizing particles. The Momentum resolution for 105 MeV electrons

is expected to be better than 180 keV/c, enough to suppress background electrons coming from the decays of muons captured by Al nuclei and from DIO.

In Figure 4 (right), an example of the first panel prototype built is shown.

One major background source for Mu2e is related to cosmic ray muons faking CEs when interacting with the detector materials. In order to reduce their contributions to below 0.1 event in the experiment lifetime, the CRV system is required to get a vetoing efficiency of at least 99.99% for cosmic ray tracks while withstanding an intense radiation environment. The basic element of the CRV is constituted by four staggered layers of scintillation bars, each having two embedded Wavelength Shifting Fibres readout by means of (2×2) mm^2 SiPM.

5 The Mu2e Calorimeter

The electromagnetic calorimeter [10] is a high granularity crystal-based calorimeter needed to:

- identify conversion electrons
- provide particle identification to suppress muons and pions faking conversion electrons
- add trigger capabilities
- add seed positioning and timing in the track reconstructions

It is composed of two annuli with inner and outer radii of 37.4 cm and 66 cm respectively, filled by pure CsI scintillating crystals and is placed downstream the tracker. Each annulus is composed of 674 crystals of $(34 \times 34 \times 200)$ mm^3 dimensions, each readout by two custom arrays of 2×3 6×6 mm^2 UV-extended Silicon Photomultiplier (SiPM); the SiPM are optimised to increase the quantum efficiency for 315 nm photons, the fast emission component of the scintillating process of CsI crystals. The granularity and crystal dimensions have been optimised to maximise light collection for readout photosensor, time and energy resolutions and take under control particles pile-up. Each crystal is wrapped with 150 μm Tyvek 4173D to maximise light collection.

In Figure 6 (left) a drawing of these two annuli is shown. Similarly to the tracker, the inner circular hole allows electrons up to 55 MeV/c momenta to escape undetected.

In Figure 6 (right) an exploded view of a single calorimeter annulus is shown.
It consists of an outer monolithyc Al cylinder that provides the main support for the crystals and integrates the feet and adjustment mechanism to park the detector on the rails inside the detector solenoid. The inner support is made of a Carbon Fiber cylinder that maximise passive material X_0. The crystals are then sandwiched between two cover plates. A Carbon Fiber front plate also integrates thin wall Al pipes to flow the radioactive Fluorinert fluid to calibrate the response; a back plate made of PEEK with apertures in correspondence of each crystals where the Front End Electronics (FEE) and SiPM holders will be inserted. The back plate houses also the Copper pipes where a coolant is flown to thermalise the photosensors and extract the power dissipated by both the FEE and the sensors. The calorimeter has to operate in the hostile experimental environment with 1 T magnetic field and a vacuum of 10^{-4} Torr, a maximum neutron fluence of 10^{12} n/cm^2 in 3 years, a maximum ionising dose of 100 krad in the hottest region at lower radii of the calorimeter.

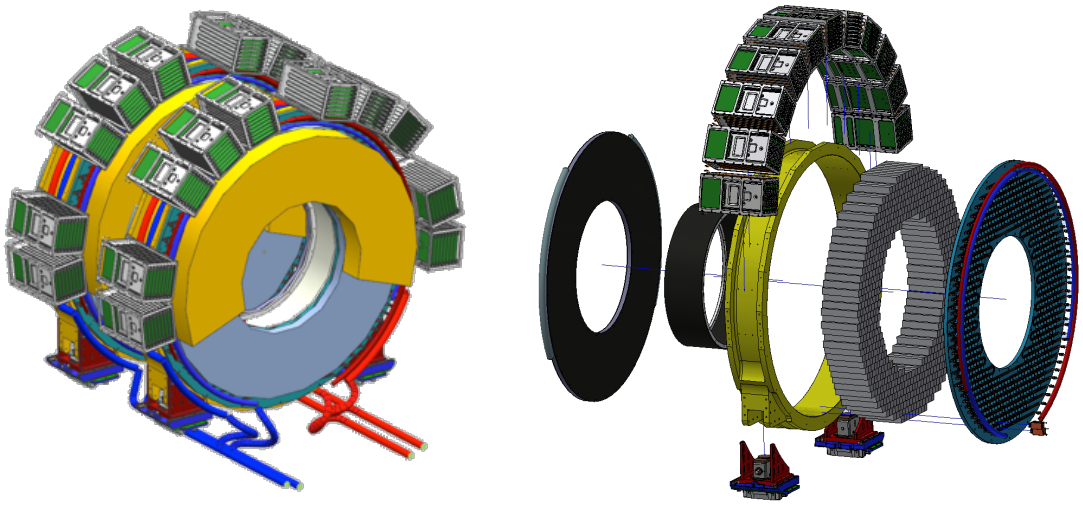

Figure 6. (Left) CAD drawings of the calorimeter disks. Calorimeter innermost (outermost) radius is of 350 mm (600 mm). Layout of the FEE and digitization crates is also shown. (Right) Exploded view of all the calorimeter parts.

10 custom made crates are arranged on top of the outer cylinder and are connected to the cooling circuit.

The calorimeter particle identification provides a good separation between CE's and muons, un-vetoed by the CRV, mimicking the signal. The required muon rejection factor (200) is achieved with 95% efficiency on the signal, combining the time of flight difference between the tracker track and the calorimeter cluster with the E/p ratio.

In order to satisfy these requirements, the calorimeter has to reach an energy resolution of O(5%), a time resolution less than 500 ps and a position resolution better than 1 cm for 100 MeV electrons. The selected crystals should also be radiation hard up to 100 krad. The photosensors are shielded by the crystals themselves and should only sustain a fluency up to 3×10^{11} n/cm^2.

5.1 Calorimeter performances and prototyping

A calorimeter prototype consisting of a 3×3 matrix of $30 \times 30 \times 200$ mm^2 un-doped CsI crystals wrapped with 150 μm Tyvek and read out by one 12×12 mm^2 SPL TSV SiPM by Hamamatsu has been tested with an electron beam at the Beam Test Facility (BTF) in Frascati during April 2015. The results, described in [8], are coherent with the ones predicted by the GEANT4 simulation [9] and are shown in Figure 7:

- time resolution better than 150 *p*s for 100 MeV electrons. The timing resolution ranges from about 250 ps at 22 MeV to about 120 ps in the energy range above 50 MeV.
- energy resolution of $\sim$ 7% for 100 MeV electrons, dominated by the shower non-containment.

We have built a Module-0 prototype composed of 51 CsI crystals from different vendors (Siccas, St. Gobain and Amcrys) instrumented with SiPM from 3 different companies (Hamamatsu, Sensl,

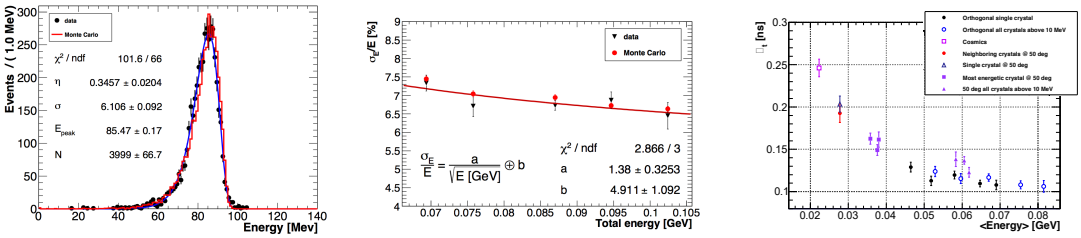

Figure 7. BTF results:(left) Data-MC comparison for energy reconstruction of 100 MeV electrons; a typical fit to the data with a log-normal function is shown in red; left long tail is due to not full containment of the shower; (center) energy resolution as a function of the reconstructed total energy; (right) time resolution as function of energy for different configurations of the matrix as function of energy.

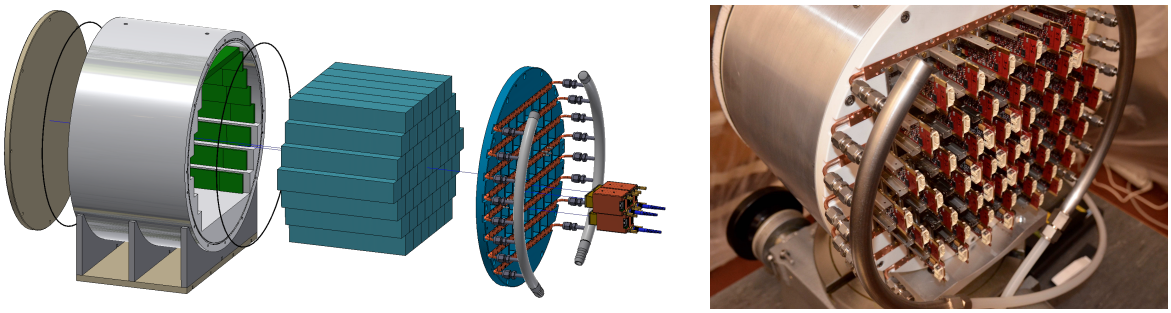

Figure 8. CAD drawing of the Module-0 (left) and its realization (right)

Advansid) to test their quality and to test the current design technological performance. Figure 8 shows the CAD drawing of the Module-0 and its actual realization. This Module-0 has been tested at the Frascati BTF and data analysis is underway.

A full scale mock-up of the mechanical structure is being built to test the assembly of the crystals, FEE electronics, cooling system and overall structure robustness : the Al outer ring, the inner Carbon Fiber cylinder, sections of the front and back plates, crate prototype have been manufactured. A whole annulus will be assembled using a mixture of fake Iron crystals and a sample of preproduction CsI crystals. Figure 9 shows the ongoing mock-up.

6 Conclusions and perspectives

The Mu2e experiment design and construction proceeds well and it is on schedule to be commissioned with beam for the end of 2021. Its goal is to probe CLFV with a single event sensitivity of 2.5×10^{-16} or set an upper limit on the conversion rate $< 6 \times 10^{-17}$ at 90 % C.L. improving of four orders of magnitude the sensitivity of previuos measurements . A Mu2e second phase is already planned with the goal of increasing the sensitivity of an additional factor of 10. The Calorimeter design is almost complete and the prototyping of the most delicate components is underway. The Module-0 construction showed a good coupling between photosensors and crystals and also the

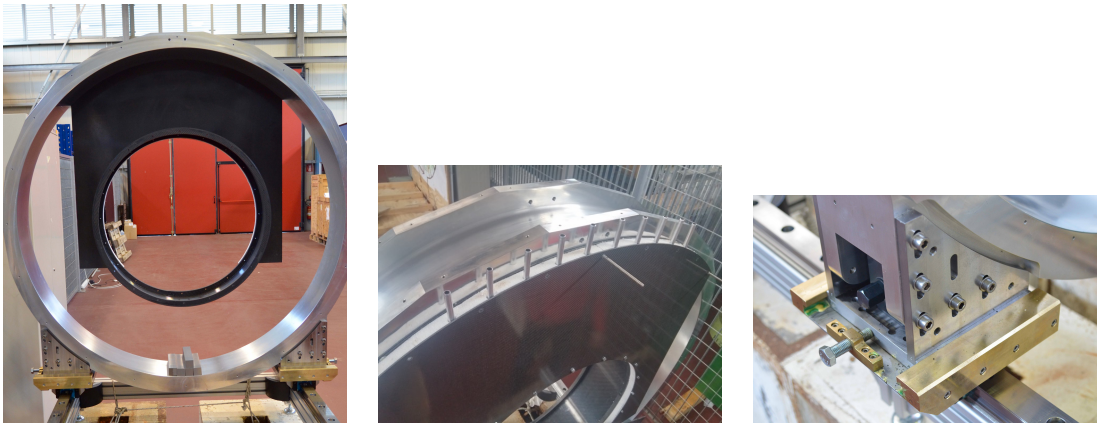

Figure 9. Full scale mock-up. Outer Al cylinder, front plate with source piping, foot with x-y adjustment.

capability to cool down the SiPM and extract heat with the current cooling scheme. We will start the construction of the final components in Year 2018 together with the opening of the tenders for crystals and SiPM purchase.

Acknowledgments

This work was supported by the EU Horizon 2020 Research and Innovation Programme under the Marie Sklodowska-Curie Grant Agreement No. 690835.

References

[1] *Mu2e Collaboration*, *http://mu2e.fnal.gov/collaboration.shtml*

[2] L. Bartoszek, et al. *Mu2e Technical Design Report*, *arXiv:1501.05241*

[3] W. Bertl et al *A search for $\mu - e$ conversion in muonic gold*, *The European Physical Journal C - Particles and Fields*47(2)2006337-346

[4] Marciano, Mori, and Roney *Flavour physics of leptons and dipole moments*, *Ann. Rev. Nucl. Sci. 58*doi:58.110707.1711262008[arXiv:0801.1826]

[5] A. De Gouvea et al. *Lepton Flavor and Number Conservation, and Physics Beyond the Standard Model*, *Prog. Part. Nucl. Phys 71,75-92*doi:10.1016/j.ppnp.2013.03.0062013arXiv:1303.4097

[6] R. Bernstein and P. Cooper *Charged Lepton Flavor Violation: An Experimenter's Guide FERMILAB-PUB-13-259-PPD*doi:10.1016/j.physrep.2013.07.0022013arXiv:1307.5787

[7] A.M. Baldini et al. *Search for the lepton flavour violating decay $\mu^+ \rightarrow \gamma\, e^+$ with the full dataset of the MEG experiment*, *Eur. Phys. J. C (2016) 76: 434* doi:10.1140/epjc/s10052-016-4271-x2016arXiv:1605.05081

[8] O. Atanova et al. *Measurement of the energy and time resolution of a undoped CsI + MPPC array for the Mu2e experiment Journal: JINST 12 (2017) P05007*

[9] S. Agostinelli et al., *Geant4: a simulation toolkit*, *NIM A, 506, 3, 250-303, 2003*.

[10] N. Atanov. et al. *Design and status of the Mu2e electromagnetic calorimeter*, *Nucl. Instr. and Meth.A 5857*doi:10.1016/j.nima..09.0742016arXiv:1608.02652